

Neighboring Zn–Zr Sites in a Metal–Organic Framework for CO₂ Hydrogenation

Jingzheng Zhang,[§] Bing An,[§] Zhe Li,[§] Yonghua Cao, Yiheng Dai, Wangyang Wang, Lingzhen Zeng, Wenbin Lin, and Cheng Wang*



Cite This: *J. Am. Chem. Soc.* 2021, 143, 8829–8837



Read Online

ACCESS |



Metrics & More

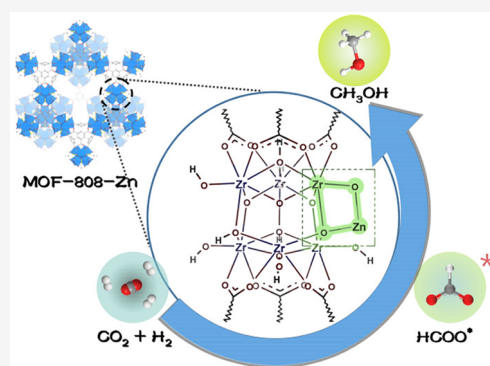


Article Recommendations



Supporting Information

ABSTRACT: ZrZnO_x is active in catalyzing carbon dioxide (CO₂) hydrogenation to methanol (MeOH) via a synergy between ZnO_x and ZrO_x. Here we report the construction of Zn²⁺–O–Zr⁴⁺ sites in a metal–organic framework (MOF) to reveal insights into the structural requirement for MeOH production. The Zn²⁺–O–Zr⁴⁺ sites are obtained by postsynthetic treatment of Zr₆(μ₃-O)₄(μ₃-OH)₄ nodes of MOF-808 by ZnEt₂ and a mild thermal treatment to remove capping ligands and afford exposed metal sites for catalysis. The resultant MOF-808-Zn catalyst exhibits >99% MeOH selectivity in CO₂ hydrogenation at 250 °C and a high space-time yield of up to 190.7 mg_{MeOH} g_{Zn}⁻¹ h⁻¹. The catalytic activity is stable for at least 100 h. X-ray absorption spectroscopy (XAS) analyses indicate the presence of Zn²⁺–O–Zr⁴⁺ centers instead of Zn_mO_n clusters. Temperature-programmed desorption (TPD) of hydrogen and H/D exchange tests show the activation of H₂ by Zn²⁺ centers. Open Zr⁴⁺ sites are also critical, as Zn²⁺ centers supported on Zr-based nodes of other MOFs without open Zr⁴⁺ sites fail to produce MeOH. TPD of CO₂ reveals the importance of bicarbonate decomposition under reaction conditions in generating open Zr⁴⁺ sites for CO₂ activation. The well-defined local structures of metal–oxo nodes in MOFs provide a unique opportunity to elucidate structural details of bifunctional catalytic centers.



INTRODUCTION

Catalytic hydrogenation of CO₂ to methanol using hydrogen from renewable sources has received much recent interest. Methanol is not only a C1 fuel but also a platform chemical for synthesizing olefins and other high value-added chemicals.^{1–6} Much progress has been made in developing supported metal catalysts for CO₂ hydrogenation. Notably, trimetallic and bimetallic catalysts such as CuZnAl, CuZr, and ZrZn have been widely studied.^{7–10} Despite the lower activity of the ZrZn catalysts than Cu-based catalysts, ZrZn catalysts have gained significant interest because of their lower cost and a lower tendency to catalyze olefin hydrogenation than Cu catalysts, which is critical for one-reactor syngas conversion to ethylene via the methanol intermediate.^{2,11,12}

ZnO was previously thought of as a promoter for Cu in CuZnAl,^{13,14} but recent studies revealed H₂ splitting and CO₂ adsorption directly on ZnO.^{3,5,10,15–17} Chen and co-workers showed that the ZnO/ZrO₂ interface of the ZrZn catalyst is the active site for CO₂ adsorption and identified a formate intermediate on both Zn and Zr metal centers.¹⁵ Li and co-workers found that Zn in the ZrO₂ lattice in a ZrZn solid solution can adsorb and split H₂ at 280 °C via H/D exchange experiments and DFT calculations.¹⁰ A Zn–O–Zr site in this solid solution then adsorbs CO₂ for its conversion to methanol as revealed by temperature-programmed desorption of CO₂

(CO₂-TPD). Our previous study on CO₂ hydrogenation using the CuZnZr catalyst found hydrogen desorption from ZnO_x by H₂-TPD.⁹ These pieces of evidence suggest that Zn is active for H₂ activation, and both Zn and Zr participate in CO₂ activation. Still, the precise chemical structures of Zn and Zr in their active forms have yet to be elucidated.

Metal–organic frameworks (MOFs),^{9,18–26} built from bridging ligands and metal–oxo cluster secondary building units (SBUs), have served as porous supports for efficient catalysts. In particular, postsynthetic modification of MOF SBUs has provided a new opportunity to study heterogeneous catalysis.^{27–35} Specifically, the μ₃-OH groups of [Zr₆(μ₃-O)₄(μ₃-OH)₄(carboxylate)₁₂] SBU in Zr-MOFs have a pK_a of 3–4 and can be deprotonated to bind other metal centers.^{26,35–38} The μ₃-O⁻ and other oxygens on the SBUs mimic the coordination environments of traditional metal oxide supports and have well-defined and uniform sites to facilitate mechanistic studies.

Received: March 31, 2021

Published: June 7, 2021



Zr SBUs have been used to support metal centers via solution-based postsynthetic modification or atomic layer deposition.^{9,29,35,36} For example, treating Zr SBUs with ZnEt₂ can deprotonate Zr₃(μ₃-OH) groups to generate Zr₃(μ₄-O)ZnEt moieties. On the other hand, capping formates on the [Zr₆(μ₃-O)₄(μ₃-OH)₄(carboxylate)₁₂] SBUs^{41–44} can decompose at the CO₂ hydrogenation temperature to generate open Zr⁴⁺ sites.^{9,39,40} We envisioned that a combination of ZnEt₂ treatment and formate removal from the SBU might afford well-defined Zn²⁺–O–Zr⁴⁺ sites for CO₂ hydrogenation to MeOH.

In this work, we synthesized MOF-808 of the formula [Zr₆(μ₃-O)₄(μ₃-OH)₄(HCO₂)₆(BTC)₂] from ZrOCl₂, benzene-tricarboxylic acid (H₃BTC), and formic acid. The capping formates were thermally removed *in situ* to generate an open Zr⁴⁺ site. The treatment of MOF-808 by ZnEt₂ afforded MOF-808-Zn as a catalyst precursor, which was highly active for CO₂ hydrogenation after a very short induction period. MOF-808-Zn showed >99% MeOH selectivity for CO₂ hydrogenation at 250 °C, a high space-time yield of up to 190.7 mg_{MeOH} g_{Zn}⁻¹ h⁻¹, and a CO₂ conversion of 2.1%. The catalytic activity was stable for at least 100 h. Further mechanistic investigations revealed that Zn²⁺ is responsible for H₂ activation and the Zn²⁺–O–Zr⁴⁺ site is critical for CO₂ adsorption and conversion.

RESULTS AND DISCUSSION

Synthesis and Characterization of MOF-808-Zn-*x*.

MOF-808 was synthesized following a modified procedure

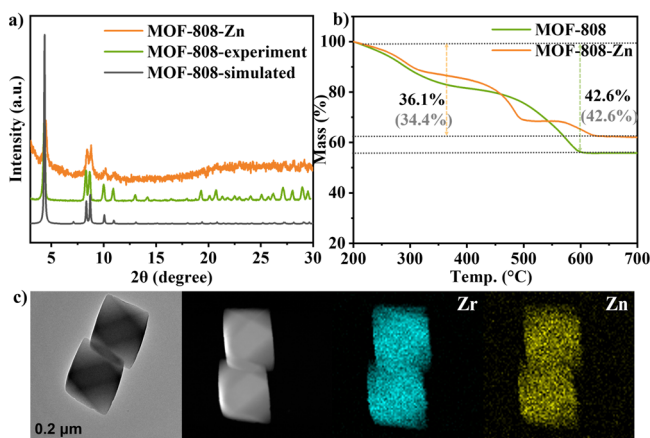


Figure 1. Characterization of MOF-808-Zn. (a) Powder X-ray diffraction patterns; (b) TGA; and (c) TEM, HADDF, and EDX mapping images of MOF-808-Zn.

using ZrOCl₂ and H₃BTC in the presence of HCO₂H (Supporting Information [section S2]).³² The resultant MOF-808 nanoparticles showed regular octahedral shape by transmission electron microscopy (TEM) (Figures 1c and S1) and were crystalline as shown by powder X-ray diffraction (PXRD) (Figure 1a). MOF-808 constructed from [Zr₆(μ₃-O)₄(μ₃-OH)₄(HCO₂)₆(carboxylate)₆] SBUs and BTC ligands have a 6,3-connected three-dimensional framework structure of *spn* topology. The number of formates was determined by proton nuclear magnetic resonance (¹H NMR) spectra of the digested MOFs, confirming the chemical formula (Figure S2). Thermogravimetric analysis (TGA) in Figure 1b gave 42.6% weight loss in the temperature range of 220–600 °C because

Scheme 1. Scheme Showing the Synthesis of MOF-808-Zn and the Active Site of Zr⁴⁺–O–Zn²⁺

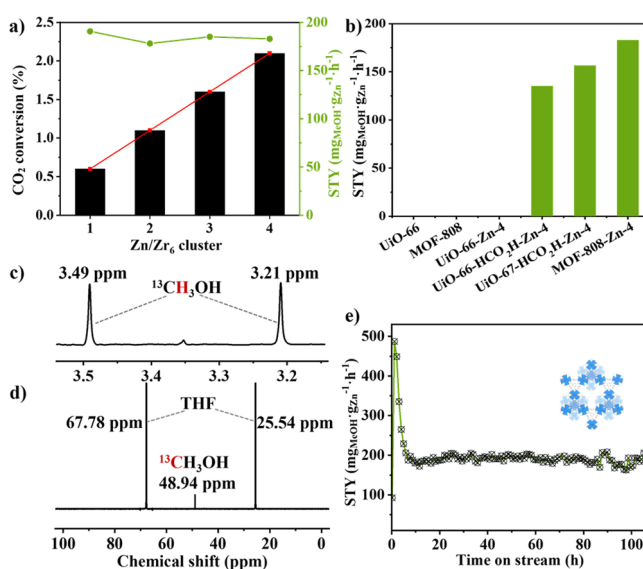
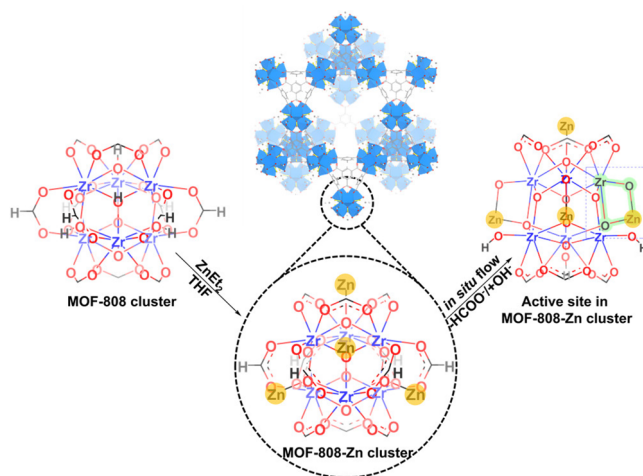


Figure 2. Catalytic performance of MOF-808-Zn-*x* (*x* = 1, 2, 3, 4). (a) Activities of MOF-808-Zn-*x* with different Zn loadings. (b) Activities of MOF-808-Zn-4 and control samples. (c) ¹H NMR and (d) ¹³C NMR of ¹³CH₃OH produced from ¹³CO₂ hydrogenation catalyzed by MOF-808-Zn-4. (e) STY_{MeOH} of MOF-808-Zn-4 vs reaction time over a period of more than 100 h on stream. Reaction conditions: GHSV = 9000 h⁻¹, temperature = 250 °C, H₂/CO₂ = 3, *P* = 4 MPa.

of conversion of Zr₆(μ₃-O)₄(μ₃-OH)₄(HCO₂)₆(BTC)₂ to ZrO₂ (theoretical weight loss: 42.6%). In the temperature range of 220–350 °C, there was about 14.4% weight loss corresponding to removing the capping formates (cal: 12.3%; Figure S3), which will be further discussed later.

MOF-808-Zn-*x* (*x* is the molar ratio of Zn/Zr₆; *x* = 1, 2, 3, 4) was synthesized by treating MOF-808 with different concentrations of ZnEt₂ in tetrahydrofuran (THF) (SI section S2.1.2, Scheme 1). The amounts of Zn and Zr were quantified by inductively coupled plasma optical emission spectroscopy (ICP-OES) and inductively coupled plasma-mass spectrometry (ICP-MS), as listed in Table S1. MOF-808-Zn-4 initially contained fully occupied Zr₆(μ₃-O)₄(μ₃-OZnEt)₄ clusters, but –OH replaced the ethyl group upon exposure to water vapor in the air to give Zr₆(μ₃-O)₄(μ₃-OZnOH)₄.

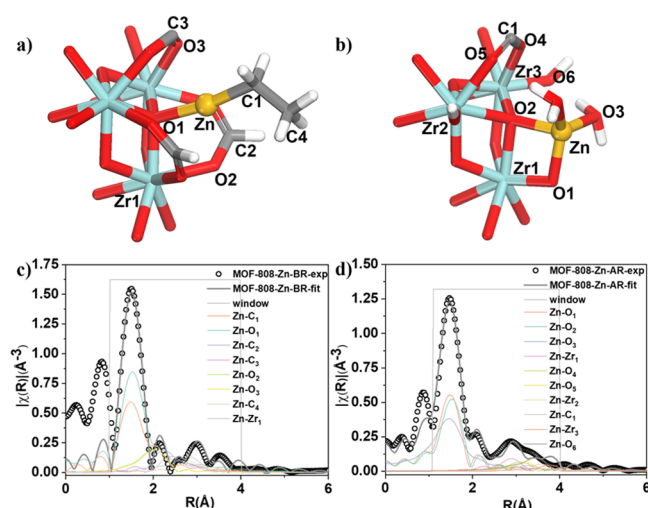


Figure 3. Local structures of (a) MOF-808-Zn-BR and (b) MOF-808-Zn-AR; R space EXAFS fitting plot of (c) MOF-808-Zn-BR and (d) MOF-808-Zn-AR. The sample before catalysis was not exposed to air for the EXAFS analysis, so there is still an ethyl group on the Zn center.

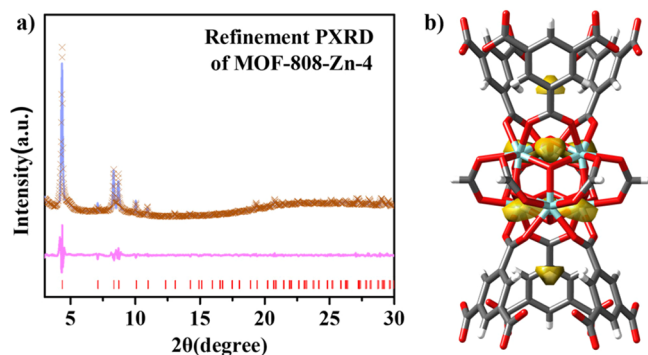


Figure 4. (a) Result of Le Bail refinements of PXRD patterns of MOF-808-Zn-4. (b) Location of Zn shown as gold area, based on “difference envelope densities” $\Delta\rho$ of MOF-808-Zn-4 minus MOF-808. Zr, turquoise; Zn, gold; C, gray; H, white.

PXRD and TEM studies showed that MOF-808-Zn- x remained crystalline (Figures 1a,c, S4, and S5). Zn distributed evenly in the framework as revealed by energy-dispersive X-ray (EDX) mapping. No ZnO or ZrO₂ nanoparticles were detected (Figure S6). After metalation with ZnEt₂, there were still six capping formates per SBU, as revealed by ¹H NMR of the digested sample (Figure S7). TGA in Figure 1b gave 36.1% weight loss in the temperature range of 220–630 °C because of the mass loss from converting Zr₆(μ₃-O)₄(μ₃-OZnOH)₄(HCO₂)₆(BTC)₂ to ZrO₂ and ZnO (theoretical mass loss: 34.4%). In the temperature range of 220–320 °C, there was about 10.4% weight loss corresponding to the capping formates’ decomposition (theoretical mass loss: 9.9%) (Figure S8). At the reaction temperature of 250 °C, the capped formate’s decomposition generated an open Zr⁴⁺ site for catalysis. Nitrogen sorption experiments gave BET surface areas of 1511 m²/g for pristine MOF-808, 831 m²/g for MOF-808-Zn-1, and 326 m²/g for MOF-808-Zn-4 (Figures S10–S15), consistent with pore-filling by the ZnOH moiety and mass increase from Zn loading.

Catalytic Performance. Catalytic Performance of MOF-808-Zn- x Reveals One Zn Center Per Active Site. MOF-808-

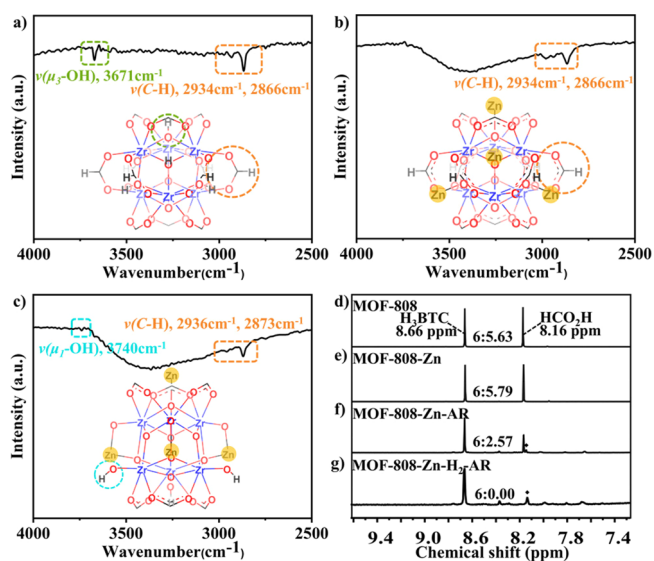


Figure 5. Infrared spectrum of (a) pristine MOF-808, (b) fresh MOF-808-Zn-4, and (c) MOF-808-Zn-4-AR. The ratio of ligand H₃BTC to HCO₂H in (d) MOF-808, (e) MOF-808-Zn-4, (f) MOF-808-Zn-4-AR (after H₂/CO₂ reaction), and (g) MOF-808-Zn-H₂-AR (after pure H₂ reduction reaction) as shown by ¹H NMR. ♦ is unknown species in panels f and g.

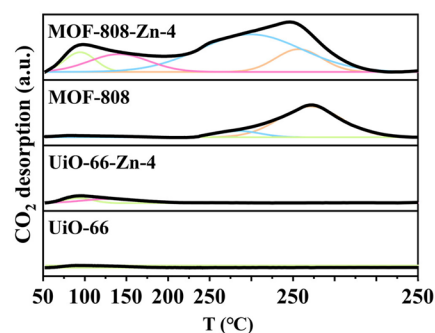


Figure 6. Normalized CO₂-TPD profiles of various MOF samples in the 50–250 °C temperature range.

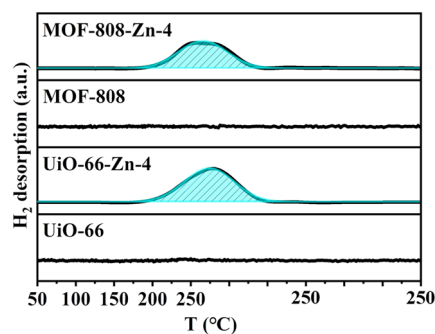


Figure 7. Normalized H₂-TPD profiles of various MOF samples in the 50–250 °C temperature range.

Zn- x ($x = 1, 2, 3, 4$) were tested for CO₂ hydrogenation at 250 °C under 4 MPa reaction gas with an H₂/CO₂ ratio of 3 on a fixed-bed reactor. MOF-808-Zn-4 exhibited a space-time yield to MeOH (STY_{MeOH}) of 182.9 mg_{MeOH} g_{Zn}⁻¹ h⁻¹ and >99% selectivity for MeOH at a gas hourly space velocity (GHSV) of 4500 h⁻¹ (Figure 2a). In comparison, the bare MOF-808 without Zn loading had no activity, reflecting the importance

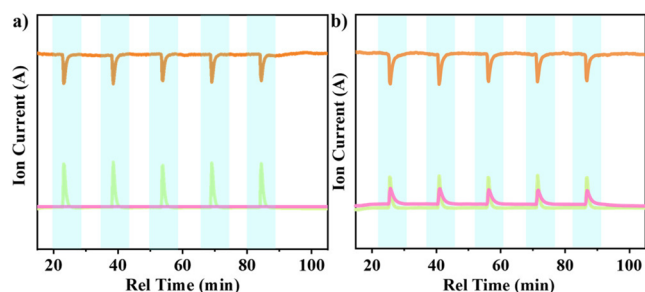


Figure 8. HD exchange profiles of (a) MOF-808 and (b) MOF-808-Zn-4. The light orange line represents $m/z = 2$; the pink line represents $m/z = 3$, and the light green line represents $m/z = 4$. The aqua color shadings suggest the deuterium gas injection interval.

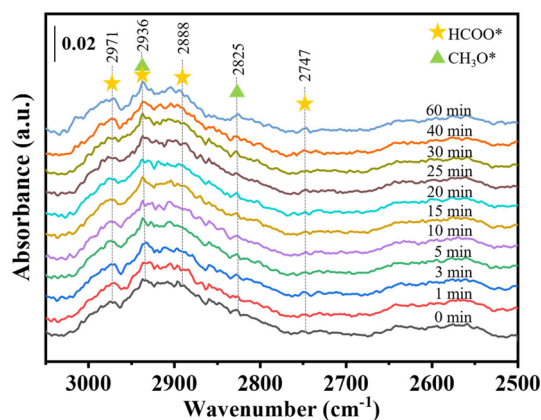


Figure 9. *In situ* DRIFT spectra of MOF-808-Zn catalyst after switching the feed gas from CO_2 to the reaction gas ($\text{H}_2/\text{CO}_2 = 3$) at 250°C and 2 MPa. The spectra are referenced to MOF-808-Zn after activation in N_2 at 250°C for 2 h.

of Zn in this catalytic reaction. The catalysts with different Zn loadings ($x = 1, 2, 3, 4$) showed similar STY_{MeOH} on a per gram of Zn basis ($x = 1:190.7 \text{ mg}_{\text{MeOH}} \text{ g}_{\text{Zn}}^{-1} \text{ h}^{-1}$; $x = 2:178.1 \text{ mg}_{\text{MeOH}} \text{ g}_{\text{Zn}}^{-1} \text{ h}^{-1}$; $x = 3:185.1 \text{ mg}_{\text{MeOH}} \text{ g}_{\text{Zn}}^{-1} \text{ h}^{-1}$; $x = 4:182.9 \text{ mg}_{\text{MeOH}} \text{ g}_{\text{Zn}}^{-1} \text{ h}^{-1}$), leading to a linear dependence of the CO_2 conversion on x (Figure 2a and Table S3). This linear dependence is consistent with an active site containing only one Zn center instead of Zn_nO_m clusters with multiple Zn centers.

MOF-808-Zn-4 showed stable catalytic performance in 100 h without a decrease in STY_{MeOH} and the selectivity (Figure 2e). The initially high activity in Figure 2e might be due to the decomposition of capping formates on the SBU, which could also be converted to MeOH. Reuse of MOF-808-Zn for a second time showed no decrease in activity. However, the initial high activity was not observed in the second run, which is consistent with our hypothesis of initial MeOH production via hydrogenating capping formates (Figure S16). Structures of MOF-808-Zn- x were maintained after catalysis as shown by PXRD patterns (Figure S17) and TEM and EDX mapping images (Figures S18 and S19) after catalysis. No sign of aggregation of Zn was observed in the TEM images.

Hydrogenation of ^{13}C -labeled $^{13}\text{CO}_2$ verified that the carbon in the CH_3OH product came from CO_2 . The reaction was performed in a high-pressure steel reactor at 250°C and under 2 MPa gas of $\text{H}_2/^{13}\text{CO}_2 = 3/1$ using MOF-808-Zn-4 as the catalyst. Gas chromatography–mass spectrometry (GC-MS) showed that $^{13}\text{CH}_3\text{OH}$ was produced with only a trace amount

of $^{12}\text{CH}_3\text{OH}$ (Figure S21). ^1H NMR analysis of the product showed splitting of the $^{13}\text{CH}_3$ - peak to a doublet peak ($\delta = 3.49 \text{ ppm}$ and $\delta = 3.21 \text{ ppm}$) due to coupling between ^{13}C and H (Figures 2c and S22). The small amount of $^{12}\text{CH}_3\text{OH}$ (3.35 ppm in Figure 2c) might be produced from the capping formate in the MOF-808-Zn cluster as mentioned above. ^{13}C NMR showed a $\delta = 48.94 \text{ ppm}$ peak assigned to $^{13}\text{CH}_3\text{OH}$ (Figure 2d).

Control Experiments Reveal the Role of Open Zr Sites. To probe the possible involvement of open Zr sites in catalytic activity, Zn supported on UiO-66 was tested for CO_2 hydrogenation.⁴⁵ The UiO-66 contains 12-connected $[\text{Zr}_6(\mu_3\text{-O})_4(\mu_3\text{-OH})_4(\text{carboxylate})_{12}]$ SBUs and terephthalate (BDC). The preparation condition of the UiO-66 was controlled to reduce the number of defect sites of formate coordination on the SBUs, and the synthesis materials were ZrCl_4 , H_2BDC , and DMF. No additional regulating agent was added. Detailed synthesis procedure and quantitative characterization of UiO-66 are presented in SI section S5.1. ^1H NMR analysis of digested UiO-66-Zn gave the BDC/formate ratio, and TGA analysis afforded the BDC/Zr ratio, both of which confirmed the presence of only a tiny amount of capping formates in this sample (0.18 formate per SBU) (Figures S26 and S29). With a minimal amount of capping formates in UiO-66, very few open Zr sites could be generated under reaction conditions. The negligible activity was observed for the UiO-66-Zn-4 catalyst (Figure 2b and Table S3) despite the formation of the $\text{Zr}_6(\mu_3\text{-O})_4(\mu_3\text{-OZnOH})_4$ cluster as in MOF-808-Zn-4, suggesting the importance of open Zr sites.

To further demonstrate the effectiveness of the open Zr site in the activity, UiO-66 with capping formates on the SBUs as defect sites were also prepared by adding HCO_2H in the synthesis (Section S5.2).⁴¹ UiO-66- HCO_2H has the same structure as UiO-66 except for the presence of capping formates. The ratio between capping formates and BDC in the UiO-66- HCO_2H was 1:1.11 according to ^1H NMR analysis (Figure S31), leading to a formula of $[\text{Zr}_6(\mu_3\text{-O})_4(\mu_3\text{-OH})_4(\text{BDC})_{4.14}(\text{HCO}_2)_{3.72}]$. After Zn loading to produce $\text{Zr}_6(\mu_3\text{-O})_4(\mu_3\text{-OZnOH})_4$ clusters, UiO-66- HCO_2H -Zn-4 was active in hydrogenating CO_2 to methanol with an STY_{MeOH} as high as $135.2 \text{ mg}_{\text{MeOH}} \text{ g}_{\text{Zn}}^{-1} \text{ h}^{-1}$ and a MeOH selectivity >99%, which is comparable to that of MOF-808-Zn-4. Similarly, UiO-67- HCO_2H with a formula of $[\text{Zr}_6(\mu_3\text{-O})_4(\mu_3\text{-OH})_4(\text{BPDC})_{5.2}(\text{HCO}_2)_{1.6}]$ was prepared. UiO-67- HCO_2H has the same structure as UiO-66- HCO_2H except that biphenylphthalic acid (H_2BPDC) is used as the bridging ligand so that the channel size of UiO-67 is larger. UiO-67- HCO_2H -Zn-4 exhibited comparable activity with an STY_{MeOH} of $156.6 \text{ mg}_{\text{MeOH}} \text{ g}_{\text{Zn}}^{-1} \text{ h}^{-1}$ with a MeOH selectivity >99%. The activity comparison among UiO-66-Zn-4, UiO-66- HCO_2H -Zn-4, and UiO-67- HCO_2H -Zn-4 highlights open Zr sites as a critical factor in CO_2 hydrogenation. We thus propose one Zn^{2+} center together with an open Zr^{4+} as the active site for catalytic CO_2 hydrogenation to methanol.

Probing the $\text{Zr}^{4+}\text{-O-Zn}^{2+}$ active site. *X-ray Absorption Spectroscopy Analysis of Zn^{2+} Coordination Environment.* The local coordination environments of Zn centers in MOF-808-Zn were probed by X-ray absorption spectroscopy (XAS) at the Zn $K\alpha$ edge (section S6.1). Fitting of extended X-ray absorption fine structure (EXAFS) (Figure 3) of the Zn K -edge of MOF-808-Zn-BR (as-synthesized, BR stands for before catalytic reaction) and MOF-808-Zn-AR (AR stands for after catalytic reaction) showed single-site Zn^{2+} centers instead of

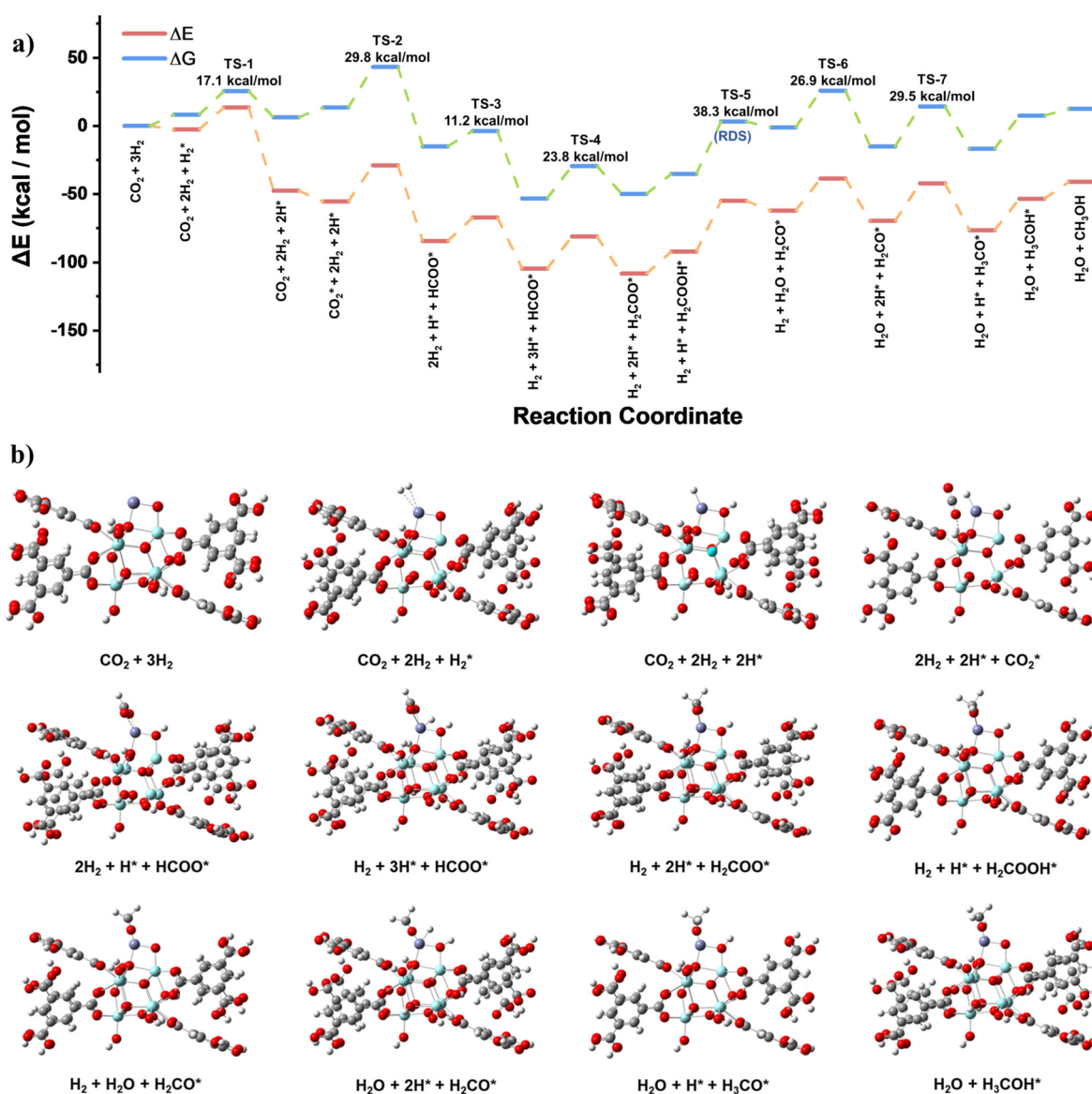


Figure 10. (a) DFT-computed minimum-energy profile on the reaction path for the catalytic hydrogenation of CO₂ to methanol on the Zr⁴⁺–O–Zn²⁺ site. (b) Related structure of the key intermediates in the catalytic cycle. The atoms in ball-and-stick models: aqua blue, Zr; red, O; gray, C; white, H; bluish violet, Zn.

forming ZnO nanoparticles or clusters. MOF-808-Zn-BR for XAS measurement was prepared in an N₂-filled glovebox, so an ethyl group from ZnEt₂ reagents is expected to coordinate the Zn²⁺ center. When exposed to air or water steam, the Zn-ethyl group was easily hydrolyzed to a ZnOH-moiety. As expected, the coordination number around Zn²⁺ in MOF-808-Zn-AR is 3.2 ± 0.8 based on the first shell EXAFS fitting. X-ray absorption near edge structure (XANES) simulation of MOF-808-Zn with different coordination numbers (CN = 2–4) (Figure S38) indicates that the four-coordinated tetrahedron structure matches best with the experimental spectrum. The proposed structure model was also confirmed by EXAFS fitting and gave the average Zn–O distance as 1.94 ± 0.03 Å, and the Zn–Zr distance around 3.01 ± 0.11 Å was also observed from the fitting. The oxidation state of Zn was +2 based on X-ray absorption near edge structure (XANES). XAS analyses of the catalysts before and after reaction are consistent with Zr⁴⁺–O–Zn²⁺ centers instead of Zn_nO_m clusters.

We also plotted the Zn K-edge EXAFS data of ZnO and Zn foil in R space in Figure S39. The comparison clearly showed that the Zn–O path in the MOF-808-Zn system is similar to that in ZnO. Instead, the MOF-808-Zn sample has a weak Zn–Zr path in the second shell, while the Zn–Zn path in ZnO is very strong. Zn foil showed only a Zn–Zn path, which did not appear in MOF-808-Zn and ZnO. This comparison shows that the Zn center in MOF-808-Zn is maintained as dispersed single sites without forming ZnO or Zn metallic nanoparticles.

Differential Electron Density Map Analysis of the Location of Zn²⁺. Analysis of PXRD patterns of MOF-808-Zn-4 (15.2% Zn loading) (Figure 4a) using a different electron density map (DED) method^{46,47} showed potential locations of the Zn²⁺ ions (Figure 4b; see section S6.2 for more details). We found increased electron density around the Zr₆ cluster in MOF-808 because of partially occupied Zn²⁺ at six sites that are each surrounded by one equatorial μ₃-O⁻ and two oxygen atoms from carboxylate of BTC, as well as at two sites above the axial μ₃-O⁻. We thus propose a structural model for MOF-

808-Zn-4 with four Zn^{2+} at these sites. Considering our control experiment of UiO-66-Zn-4, we assume that only Zn^{2+} at the six equatorial sites can form active centers for MeOH production.

IR Spectra Probe the Formation of the HO–Zr⁴⁺–O–Zn²⁺ Active Site. We hypothesize that the capping formate in $[\text{Zr}_6(\mu_3\text{-O})_4(\mu_3\text{-OH})_4(\text{HCO}_2)_6(\text{carboxylate})_6]$ SBUs could decompose and be replaced by H_2O and OH^- during the reaction, which can be verified by comparing the infrared (IR) absorption spectrum of MOF-808 before and after heating (Figure S4a). Two peaks at 2866 and 2934 cm^{-1} were detected in pristine MOF-808 but were absent in the sample after heating at 250 °C for 20 h (Figure S42).^{9,34,48} These two peaks can be assigned to $\nu(\text{C-H})$ stretching mode and $\delta(\text{C-H}) + \nu_{\text{as}}(\text{OCO})$ of the coordinated formate. The IR spectra of MOF-808-Zn-4 before and after catalysis showed that the $\nu(\mu_3\text{-OH})$ at 3671 cm^{-1} disappeared after metalation with ZnEt_2 (Figure S4b). A broad peak in the 3000–3600 cm^{-1} suggests adsorbed water on Zn^{2+} with rich hydrogen bonds. The $\nu(\mu_3\text{-OH})$ was also absent in the sample after catalysis (Figure S4c), indicating that Zn^{2+} stays on the $\mu_3\text{-O}^-$ site during the catalytic process. The $\nu(\mu_1\text{-OH})$ peak at 3740 cm^{-1} ^{19,49,50} was present in the MOF-808-Zn-4-AR spectrum, consistent with a left $\mu_1\text{-OH}$ on Zr^{4+} after formate removal.

Formate removal after heating was also confirmed by ¹H NMR analysis after digesting the MOFs by D_3PO_4 (Figure S43). The ratio of $\text{BTC}/\text{HCO}_2^-$ in MOF-808 is approximately 2:5.63 (Figure S4d), which did not change after metalation with ZnEt_2 (2:5.79, Figure S4e). After heating MOF-808-Zn-4 to 250 °C under 4 MPa of pure H_2 in a high-pressure steel reactor, the ¹H NMR analysis showed a negligible amount of HCO_2^- left in the MOF (Figures S4g and S45).

However, after catalysis at 250 °C under 4 MPa of $\text{H}_2/\text{CO}_2 = 3/1$, this $\text{BTC}/\text{HCO}_2^-$ ratio became 2:2.57 (Figure S4f). The IR spectra also showed a formate signal after catalysis (Figure S4c). The restored formate under CO_2 hydrogenation condition suggests that formate is a critical intermediate in the CO_2 conversion.

CO_2 -TPD Reveals CO_2 Adsorption Sites and HCO_3^- Decomposition. Chemisorption of CO_2 on the catalysts was investigated by temperature-programmed desorption of CO_2 (CO_2 -TPD). The temperature was ramped from 50 to 250 °C at a rate of 5 °C/min and then held at 250 °C for 60 min. The signal was monitored and recorded by a mass spectrometer. The CO_2 -TPD profile of MOF-808-Zn-4 was deconvoluted into four peaks: 94 °C (green), 143 °C (pink), and holding at 250 °C for 9.6 min (blue) and 25.7 min (orange) (Figure 6). The desorption peak at 94 °C was assigned to CO_2 desorption from the Zn^{2+} site, as it was also observed in the CO_2 -TPD profile of UiO-66-Zn-4 that lacks open Zr sites. This assignment is also consistent with the literature report of the CO_2 -TPD profile of ZnO .^{10,16} The two peaks at >250 °C are assigned to desorption from open Zr sites on the SBU as they also appeared in the CO_2 -TPD profile of MOF-808 without Zn metalation. However, the desorption peak at 9.6 min was much higher for MOF-808-Zn-4 than that for MOF-808, suggesting that Zn^{2+} promotes CO_2 adsorption on Zr^{4+} .⁹ The desorption peak at 143 °C is a new peak that is assigned to desorption from the $\text{Zr}^{4+}\text{-O-Zn}^{2+}$ site as it is absent in either UiO-66-Zn-4 or MOF-808 without Zn metalation.^{3,5}

Because the capping formate of MOF-808-Zn-4 decomposed before reaching 250 °C and should leave a Zr-OH , the two desorption peaks at 250 °C might be attributed to

bicarbonate species (HCO_3^-) adsorbed on the Zr site resulting from the reaction between CO_2 and Zr-OH . This assignment is consistent with literature results^{51,52} suggesting that slow decomposition of bicarbonate releases CO_2 for the observed desorption. Similarly, the first desorption peak at 94 °C in the CO_2 -TPD curve is possibly caused by the decomposition of bicarbonate species adsorbed at the Zn^{2+} site. The second peak at 143 °C possibly corresponds to HCO_3^- on the $\text{Zr}^{4+}\text{-O-Zn}^{2+}$ site.

To test this hypothesis, MOF-808 was suspended in CO_2 -saturated KHCO_3 solution overnight with continuous stirring to obtain MOF-808-HCO_3^- . The samples after sufficient washing and drying were examined by TGA-MS (Figure S46). The trace with an m/z value of 44 monitors CO_2 generation, and the trace with an m/z value of 18 monitors H_2O . When the temperature increased to ~250 °C, both CO_2 and H_2O 's mass signal appeared, suggesting the decomposition of HCO_3^- . This observation is consistent with the CO_2 -TPD data.

Notably, the temperatures at which HCO_3^- decomposed correlate with the rise of catalytic activity. We thus propose that the desorption of HCO_3^- from Zr sites may generate open Zr sites for CO_2 activation and catalytic turnover.

H_2 -TPD and H/D Exchange Experiment Showing H_2 Activation at the Zn Site. The temperature in the H_2 -TPD measurement increased from 50 to 250 °C at a rate of 5 °C/min and was then held at 250 °C for 60 min. Both MOF-808-Zn-4 with open Zr sites and UiO-66-Zn-4 without open Zr sites showed a broad desorption peak at 250 °C after holding for 5 min (Figure 7). In comparison, the MOF-808 or UiO-66 without Zn metalation showed no desorption peak of H_2 , suggesting that the Zn site is responsible for H_2 activation.

H/D exchange experiments further supported the role of the Zn site in H_2 activation. MS monitored the D_2 injection into H_2 flow in 10 min intervals at 250 °C. The m/z value of 3 is for HD produced via the reaction between H_2 and D_2 on the catalytic site. Both MOF-808-Zn-4 and UiO-66-Zn-4 produced HD, while MOF-808 without Zn metalation produced a negligible amount of HD (Figures 8 and S48), confirming the Zn site to be the one for H_2 activation.

We envisioned that the Zn^{2+} and a surrounding oxygen O site might form a Lewis acid–base pair for heterolytic H_2 splitting to generate $\text{Zn-H}^{\delta-}$ and $\text{O-H}^{\delta+}$. As the MOF-808-Zn-4 and UiO-66-Zn-4 showed similar H/D exchange activity, the suitable O site must be present in both samples. One candidate is a carboxyl oxygen atom from the BTC ligand. Other candidates include a $\mu_1\text{-OH}$ attached to the Zn^{2+} center and the $\mu_2\text{-O}$ in $\text{Zr}^{4+}\text{-O-Zn}^{2+}$.

In Situ DRIFT Revealing Reaction Intermediates. Figure 9 shows the *in situ* DRIFT spectra of MOF-808-Zn catalyst after switching the feed gas from CO_2 to the reaction gas ($\text{H}_2/\text{CO}_2 = 3; 2 \text{ MPa}$) at 250 °C. The bands at 2971, 2936, and 2888 cm^{-1} were assigned to the HCOO-Zr species (HCOO is formate)⁵¹ that exist before the switching. Upon switching to the reaction gas, the peak at 2747 cm^{-1} gradually increased with time, corresponding to the formation of HCOO-Zn species.^{53–55} The peaks at 2970 and 2888 cm^{-1} were also assigned to HCOO-Zn . It is difficult to distinguish between HCOO-Zn and formate group bridging one Zn and one Zr center. Meanwhile, the bands at 2936 and 2825 cm^{-1} increased with time, corresponding to the methanol synthesis from the formate species.^{56,57} Thus, we observed HCOO-Zn as a possible reaction intermediate.

DFT Calculations. To further investigate the reaction mechanisms, density functional theory (DFT) calculations were performed. The MOF-808-Zn cluster structure was first optimized as shown in Figure S50. This structural model is consistent with EXAFS fitting.

We have calculated the reaction process from CO₂ to methanol on the MOF-808-Zn catalyst, and the related energy change profile is shown in Figures 10 and S52. The calculations showed that H₂ is activated on the Zn²⁺ center, CO₂ is adsorbed on the Zr⁴⁺ center, and formate is a crucial intermediate.

H₂ can easily dissociate to form Zn²⁺-H⁻ and Zr⁴⁺-O-H⁺ species on the Zr⁴⁺-O-Zn²⁺ center [Zr⁴⁺-O(-H⁺)-Zn²⁺-H⁻] with an energy barrier of 17.1 kcal/mol. Then, H₂ can also be dissociated by the Zn²⁺ center and another nearby Zr⁴⁺-OH group, enabling the formation of the H₂ + 3H* + HCOO* intermediate. The barrier for H₂ splitting in this step is lower than that on Zr⁴⁺-O-Zn²⁺ (11.2 vs 17.1 kcal/mol). The change of the surrounding environment after the first hydrogen dissociation may cause this decrease. These results are consistent with the hypothesis of heterolytic H₂ splitting on Zn²⁺ and the oxygen bonded to Zr⁴⁺.

CO₂ has an adsorption enthalpy of 10.9 kcal/mol on the open Zr site. The adsorbed CO₂ reacts with the nearby Zn²⁺-H⁻ to form formate. In the catalytic cycle, all the oxygenated intermediates were adsorbed on the Zn²⁺ center. Hydride species on the same Zn²⁺ center hydrogenated them, consistent with previous studies of the ZrO₂/ZnO system.¹⁵ The high hydricity of the Zn-H^{δ-} species leads to low barriers of hydrogenating steps (23.7–29.8 kcal/mol). The rate-determining step in the cycle is the cleavage of the C–O bond in H₂CO–OH* with a barrier of 38.3 kcal/mol. This explains why formate can be observed as an intermediate, as formate is one of the stable species on the path before C–O cleavage.

The last methoxy protonation and MeOH desorption steps are both thermodynamically unfavorable but with only small barriers (24.3 and 4.9 kcal/mol, respectively).

The reaction pathway on pristine MOF-808 was also computed and compared with that of MOF-808-Zn. As shown in Figure S53, the barrier for heterolytic hydrogen splitting on the Zr–OH site was 35.8 kcal/mol, which is much higher than that on the Zn–O–Zr center in MOF-808-Zn (17.2 kcal/mol). Meanwhile, the Zr–H generation from H₂ is thermodynamically unfavorable (28.6 kcal/mol), while the enthalpy for Zn–H formation is –1.9 kcal/mol. Thus, the formation of Zr–H is both kinetically and thermodynamically unfavorable compared to the formation of Zn–H.

CONCLUSION

We constructed well-defined Zn²⁺/Zr⁴⁺ sites that are adjacent to each other in MOF-808. Zn²⁺ was loaded onto the SBU via deprotonation of a μ₃-OH with ZnEt₂. Capping formate in the Zr₆(μ₃-O)₄(μ₃-OH)₄(HCO₂)₆ SBU decomposed *in situ* to generate open Zr⁴⁺ sites. The Zr⁴⁺-O-Zn²⁺ open site is responsible for CO₂ hydrogenation to methanol. MOF-808-Zn catalyst showed >99% MeOH selectivity in CO₂ hydrogenation at 250 °C and exhibited excellent stability for at least 100 h. Mechanistic investigations revealed that Zn²⁺ is responsible for H₂ activation and the Zn²⁺-O-Zr⁴⁺ site is critical for CO₂ adsorption and conversion. The well-defined local structure around the MOF SBU provides a unique

opportunity to reveal the structural requirement for synergistic catalysis.

ASSOCIATED CONTENT

Supporting Information

The Supporting Information is available free of charge at <https://pubs.acs.org/doi/10.1021/jacs.1c03283>.

General experimental methods; preparation and characterization of catalysts; catalysis, including the testing process and additional catalytic data; TEM images of catalysts before and after reactions; and DFT calculations (PDF)

AUTHOR INFORMATION

Corresponding Author

Cheng Wang – Collaborative Innovation Center of Chemistry for Energy Materials, State Key Laboratory of Physical Chemistry of Solid Surfaces, Department of Chemistry, College of Chemistry and Chemical Engineering, Xiamen University, Xiamen 361005, P.R. China; orcid.org/0000-0002-7906-8061; Email: wangchengxmu@xmu.edu.cn

Authors

Jingzheng Zhang – Collaborative Innovation Center of Chemistry for Energy Materials, State Key Laboratory of Physical Chemistry of Solid Surfaces, Department of Chemistry, College of Chemistry and Chemical Engineering, Xiamen University, Xiamen 361005, P.R. China

Bing An – Collaborative Innovation Center of Chemistry for Energy Materials, State Key Laboratory of Physical Chemistry of Solid Surfaces, Department of Chemistry, College of Chemistry and Chemical Engineering, Xiamen University, Xiamen 361005, P.R. China

Zhe Li – Collaborative Innovation Center of Chemistry for Energy Materials, State Key Laboratory of Physical Chemistry of Solid Surfaces, Department of Chemistry, College of Chemistry and Chemical Engineering, Xiamen University, Xiamen 361005, P.R. China

Yonghua Cao – Collaborative Innovation Center of Chemistry for Energy Materials, State Key Laboratory of Physical Chemistry of Solid Surfaces, Department of Chemistry, College of Chemistry and Chemical Engineering, Xiamen University, Xiamen 361005, P.R. China

Yiheng Dai – Collaborative Innovation Center of Chemistry for Energy Materials, State Key Laboratory of Physical Chemistry of Solid Surfaces, Department of Chemistry, College of Chemistry and Chemical Engineering, Xiamen University, Xiamen 361005, P.R. China

Wangyang Wang – Collaborative Innovation Center of Chemistry for Energy Materials, State Key Laboratory of Physical Chemistry of Solid Surfaces, Department of Chemistry, College of Chemistry and Chemical Engineering, Xiamen University, Xiamen 361005, P.R. China

Lingzhen Zeng – Collaborative Innovation Center of Chemistry for Energy Materials, State Key Laboratory of Physical Chemistry of Solid Surfaces, Department of Chemistry, College of Chemistry and Chemical Engineering, Xiamen University, Xiamen 361005, P.R. China

Wenbin Lin – Department of Chemistry, University of Chicago, Chicago, Illinois 60637, United States; orcid.org/0000-0001-7035-7759

Complete contact information is available at:

<https://pubs.acs.org/10.1021/jacs.1c03283>

Author Contributions

[§]J.Z., B.A., and Z.L. contributed equally to this work.

Notes

The authors declare no competing financial interest.

ACKNOWLEDGMENTS

We acknowledge funding support from the National Natural Science Foundation and Ministry of Science and Technology of the P. R. China (NSFC 22071207, NSFC 21721001, and 2016YFA0200702).

REFERENCES

- (1) Tian, P.; Wei, Y.; Ye, M.; Liu, Z. Methanol to Olefins (MTO): From Fundamentals to Commercialization. *ACS Catal.* **2015**, *5* (3), 1922–1938.
- (2) Cheng, K.; Gu, B.; Liu, X.; Kang, J.; Zhang, Q.; Wang, Y. Direct and Highly Selective Conversion of Synthesis Gas into Lower Olefins: Design of a Bifunctional Catalyst Combining Methanol Synthesis and Carbon-Carbon Coupling. *Angew. Chem., Int. Ed.* **2016**, *55* (15), 4725–4728.
- (3) Li, Z.; Wang, J.; Qu, Y.; Liu, H.; Tang, C.; Miao, S.; Feng, Z.; An, H.; Li, C. Highly Selective Conversion of Carbon Dioxide to Lower Olefins. *ACS Catal.* **2017**, *7*, 8544–8548.
- (4) Yarulina, I.; Chowdhury, A. D.; Meirer, F.; Weckhuysen, B. M.; Gascon, J. Recent trends and fundamental insights in the methanol-to-hydrocarbons process. *Nat. Catal.* **2018**, *1* (6), 398–411.
- (5) Zhou, C.; Shi, J.; Zhou, W.; Cheng, K.; Zhang, Q.; Kang, J.; Wang, Y. Highly Active ZnO-ZrO₂ Aerogels Integrated with H-ZSM-5 for Aromatics Synthesis from Carbon Dioxide. *ACS Catal.* **2020**, *10*, 302–310.
- (6) Arstad, B.; Kolboe, S. The Reactivity of Molecules Trapped within the SAPO-34 Cavities in the Methanol-to-Hydrocarbons Reaction. *J. Am. Chem. Soc.* **2001**, *123* (33), 8137–8138.
- (7) Behrens, M.; Studt, F.; Kasatkin, I.; Kuehl, S.; Haevecker, M.; Abild-Pedersen, F.; Zander, S.; Girgsdies, F.; Kurr, P.; Knief, B.-L.; Tovar, M.; Fischer, R. W.; Norskov, J. K.; Schloegl, R. The Active Site of Methanol Synthesis over Cu/ZnO/Al₂O₃ Industrial Catalysts. *Science* **2012**, *336* (6083), 893–897.
- (8) Tada, S.; Kayamori, S.; Honma, T.; Kamei, H.; Nariyuki, A.; Kon, K.; Toyao, T.; Shimizu, K.-i.; Satokawa, S. Design of Interfacial Sites between Cu and Amorphous ZrO₂ Dedicated to CO₂-to-Methanol Hydrogenation. *ACS Catal.* **2018**, *8* (9), 7809–7819.
- (9) An, B.; Zhang, J.; Cheng, K.; Ji, P.; Wang, C.; Lin, W. Confinement of Ultrasmall Cu/ZnO_x Nanoparticles in Metal-Organic Frameworks for Selective Methanol Synthesis from Catalytic Hydrogenation of CO₂. *J. Am. Chem. Soc.* **2017**, *139* (10), 3834–3840.
- (10) Wang, J.; Li, G.; Li, Z.; Tang, C.; Feng, Z.; An, H.; Liu, H.; Liu, T.; Li, C. A highly selective and stable ZnO-ZrO₂ solid solution catalyst for CO₂ hydrogenation to methanol. *Sci. Adv.* **2017**, *3*, e1701290.
- (11) Fujiwara, M.; Souma, Y. Hydrocarbon synthesis from carbon dioxide and hydrogen over Cu–Zn–Cr oxide/zeolite hybrid catalysts. *J. Chem. Soc., Chem. Commun.* **1992**, No. 10, 767–768.
- (12) Park, Y.-K.; Park, K.-C.; Ihm, S.-K. Hydrocarbon synthesis through CO₂ hydrogenation over CuZnO/ZrO₂/zeolite hybrid catalysts. *Catal. Today* **1998**, *44* (1), 165–173.
- (13) Fichtl, M. B.; Schlereth, D.; Jacobsen, N.; Kasatkin, I.; Schumann, J.; Behrens, M.; Schlögl, R.; Hinrichsen, O. Kinetics of deactivation on Cu/ZnO/Al₂O₃ methanol synthesis catalysts. *Appl. Catal., A* **2015**, *502*, 262–270.
- (14) Xiao, J.; Mao, D.; Guo, X.; Yu, J. Effect of TiO₂, ZrO₂, and TiO₂-ZrO₂ on the performance of CuO-ZnO catalyst for CO₂ hydrogenation to methanol. *Appl. Surf. Sci.* **2015**, *338*, 146–153.
- (15) Wang, Y.; Kattel, S.; Gao, W.; Li, K.; Liu, P.; Chen, J. G.; Wang, H. Exploring the ternary interactions in Cu-ZnO-ZrO₂ catalysts for efficient CO₂ hydrogenation to methanol. *Nat. Commun.* **2019**, *10* (1), 1166.
- (16) Li, W.; Wang, K.; Huang, J.; Liu, X.; Fu, D.; Huang, J.; Li, Q.; Zhan, G. M_xO_y-ZrO₂ (M = Zn, Co, Cu) Solid Solutions Derived from Schiff Base-Bridged UiO-66 Composites as High-Performance Catalysts for CO₂ Hydrogenation. *ACS Appl. Mater. Interfaces* **2019**, *11* (36), 33263–33272.
- (17) Xaba, B. S.; Mahomed, A. S.; Friedrich, H. B. The effect of CO₂ and H₂ adsorption strength and capacity on the performance of Ga and Zr modified Cu-Zn catalysts for CO₂ hydrogenation to methanol. *J. Environ. Chem. Eng.* **2021**, *9* (1), 104834.
- (18) Wang, C.; An, B.; Lin, W. Metal-Organic Frameworks in Solid-Gas Phase Catalysis. *ACS Catal.* **2019**, *9* (1), 130–146.
- (19) Xie, L. S.; Skorupskii, G.; Dincă, M. Electrically Conductive Metal-Organic Frameworks. *Chem. Rev.* **2020**, *120*, 8536–8580.
- (20) Song, Y.; Li, Z.; Zhu, Y.; Feng, X.; Chen, J. S.; Kaufmann, M.; Wang, C.; Lin, W. Titanium Hydroxide Secondary Building Units in Metal-Organic Frameworks Catalyze Hydrogen Evolution under Visible Light. *J. Am. Chem. Soc.* **2019**, *141* (31), 12219–12223.
- (21) Yang, D.; Gaggioli, C. A.; Ray, D.; Babucci, M.; Gagliardi, L.; Gates, B. C. Tuning Catalytic Sites on Zr₆O₈ Metal-Organic Framework Nodes via Ligand and Defect Chemistry Probed with tert-Butyl Alcohol Dehydration to Isobutylene. *J. Am. Chem. Soc.* **2020**, *142* (17), 8044–8056.
- (22) Cai, Z.; Dai, J.; Li, W.; Tan, K. B.; Huang, Z.; Zhan, G.; Huang, J.; Li, Q. Pd Supported on MIL-68(In)-Derived In₂O₃ Nanotubes as Superior Catalysts to Boost CO₂ Hydrogenation to Methanol. *ACS Catal.* **2020**, *10* (22), 13275–13289.
- (23) Wang, T.; Gao, L.; Hou, J.; Herou, S. J. A.; Griffiths, J. T.; Li, W.; Dong, J.; Gao, S.; Titirici, M.-M.; Kumar, R. V.; Cheetham, A. K.; Bao, X.; Fu, Q.; Smoukov, S. K. Rational approach to guest confinement inside MOF cavities for low-temperature catalysis. *Nat. Commun.* **2019**, *10* (1), 1340.
- (24) Trickett, C. A.; Osborn Popp, T. M.; Su, J.; Yan, C.; Weisberg, J.; Huq, A.; Urban, P.; Jiang, J.; Kalmutzki, M. J.; Liu, Q.; Baek, J.; Head-Gordon, M. P.; Somorjai, G. A.; Reimer, J. A.; Yaghi, O. M. Identification of the strong Bronsted acid site in a metal-organic framework solid acid catalyst. *Nat. Chem.* **2019**, *11* (2), 170–176.
- (25) An, B.; Zeng, L.; Jia, M.; Li, Z.; Lin, Z.; Song, Y.; Zhou, Y.; Cheng, J.; Wang, C.; Lin, W. Molecular Iridium Complexes in Metal-Organic Frameworks Catalyze CO₂ Hydrogenation via Concerted Proton and Hydride Transfer. *J. Am. Chem. Soc.* **2017**, *139* (49), 17747–17750.
- (26) Diercks, C. S.; Liu, Y.; Cordova, K. E.; Yaghi, O. M. The role of reticular chemistry in the design of CO₂ reduction catalysts. *Nat. Mater.* **2018**, *17* (4), 301–307.
- (27) Song, Y.; Feng, X.; Chen, J. S.; Brzezinski, C.; Xu, Z.; Lin, W. Multistep Engineering of Synergistic Catalysts in a Metal-Organic Framework for Tandem C–O Bond Cleavage. *J. Am. Chem. Soc.* **2020**, *142* (10), 4872–4882.
- (28) Chen, X.; Lyu, Y.; Wang, Z.; Qiao, X.; Gates, B. C.; Yang, D. Tuning Zr₁₂O₂₂ Node Defects as Catalytic Sites in the Metal-Organic Framework hcp UiO-66. *ACS Catal.* **2020**, *10* (5), 2906–2914.
- (29) Li, Z.; Peters, A. W.; Bernales, V.; Ortuño, M. A.; Schweitzer, N. M.; DeStefano, M. R.; Gallington, L. C.; Platero-Prats, A. E.; Chapman, K. W.; Cramer, C. J.; Gagliardi, L.; Hupp, J. T.; Farha, O. K. Metal-Organic Framework Supported Cobalt Catalysts for the Oxidative Dehydrogenation of Propane at Low Temperature. *ACS Cent. Sci.* **2017**, *3* (1), 31–38.
- (30) Song, Y.; Li, Z.; Ji, P.; Kaufmann, M.; Feng, X.; Chen, J. S.; Wang, C.; Lin, W. Metal-Organic Framework Nodes Support Single-Site Nickel(II) Hydride Catalysts for the Hydrogenolysis of Aryl Ethers. *ACS Catal.* **2019**, *9* (2), 1578–1583.
- (31) Otake, K.-i.; Ye, J.; Mandal, M.; Islamoglu, T.; Buru, C. T.; Hupp, J. T.; Delferro, M.; Truhlar, D. G.; Cramer, C. J.; Farha, O. K. Enhanced Activity of Heterogeneous Pd(II) Catalysts on Acid-

Functionalized Metal-Organic Frameworks. *ACS Catal.* **2019**, *9* (6), 5383–5390.

(32) Baek, J.; Rungtaweevoranit, B.; Pei, X.; Park, M.; Fakra, S. C.; Liu, Y.-S.; Matheu, R.; Alshimmiri, S. A.; Alshehri, S.; Trickett, C. A.; Somorjai, G. A.; Yaghi, O. M. Bioinspired Metal-Organic Framework Catalysts for Selective Methane Oxidation to Methanol. *J. Am. Chem. Soc.* **2018**, *140* (51), 18208–18216.

(33) Feng, X.; Song, Y.; Li, Z.; Kaufmann, M.; Pi, Y.; Chen, J. S.; Xu, Z.; Li, Z.; Wang, C.; Lin, W. Metal-Organic Framework Stabilizes a Low-Coordinate Iridium Complex for Catalytic Methane Borylation. *J. Am. Chem. Soc.* **2019**, *141* (28), 11196–11203.

(34) An, B.; Li, Z.; Song, Y.; Zhang, J.; Zeng, L.; Wang, C.; Lin, W. Cooperative copper centres in a metal-organic framework for selective conversion of CO₂ to ethanol. *Nat. Catal.* **2019**, *2*, 709–717.

(35) Manna, K.; Ji, P.; Lin, Z.; Greene, F. X.; Urban, A.; Thacker, N. C.; Lin, W. Chemoselective single-site Earth-abundant metal catalysts at metal-organic framework nodes. *Nat. Commun.* **2016**, *7* (1), 12610.

(36) Yang, D.; Odoh, S. O.; Wang, T. C.; Farha, O. K.; Hupp, J. T.; Cramer, C. J.; Gagliardi, L.; Gates, B. C. Metal-Organic Framework Nodes as Nearly Ideal Supports for Molecular Catalysts: NU-1000 and UiO-66-Supported Iridium Complexes. *J. Am. Chem. Soc.* **2015**, *137* (23), 7391–7396.

(37) Marshall, R. J.; Forgan, R. S. Postsynthetic Modification of Zirconium Metal-Organic Frameworks. *Eur. J. Inorg. Chem.* **2016**, *2016* (27), 4310–4331.

(38) Klet, R. C.; Liu, Y.; Wang, T. C.; Hupp, J. T.; Farha, O. K. Evaluation of Bronsted acidity and proton topology in Zr- and Hf-based metal-organic frameworks using potentiometric acid-base titration. *J. Mater. Chem. A* **2016**, *4* (4), 1479–1485.

(39) Ji, P.; Feng, X.; Oliveres, P.; Li, Z.; Murakami, A.; Wang, C.; Lin, W. Strongly Lewis Acidic Metal-Organic Frameworks for Continuous Flow Catalysis. *J. Am. Chem. Soc.* **2019**, *141* (37), 14878–14888.

(40) Yang, K.; Jiang, J. Computational design of a metal-based frustrated Lewis pair on defective UiO-66 for CO₂ hydrogenation to methanol. *J. Mater. Chem. A* **2020**, *8* (43), 22802–22815.

(41) Gutov, O. V.; Hevia, M. G.; Escudero-Adan, E. C.; Shafir, A. Metal-Organic Framework (MOF) Defects under Control: Insights into the Missing Linker Sites and Their Implication in the Reactivity of Zirconium-Based Frameworks. *Inorg. Chem.* **2015**, *54* (17), 8396–8400.

(42) Vermoortele, F.; Bueken, B.; Le Bars, G.; Van de Voorde, B.; Vandichel, M.; Houthoofd, K.; Vimont, A.; Daturi, M.; Waroquier, M.; Van Speybroeck, V.; Kirschhock, C.; De Vos, D. E. Synthesis Modulation as a Tool To Increase the Catalytic Activity of Metal-Organic Frameworks: The Unique Case of UiO-66(Zr). *J. Am. Chem. Soc.* **2013**, *135* (31), 11465–11468.

(43) Wu, H.; Chua, Y. S.; Krungleviciute, V.; Tyagi, M.; Chen, P.; Yildirim, T.; Zhou, W. Unusual and Highly Tunable Missing-Linker Defects in Zirconium Metal-Organic Framework UiO-66 and Their Important Effects on Gas Adsorption. *J. Am. Chem. Soc.* **2013**, *135* (28), 10525–10532.

(44) Bueken, B.; Reinsch, H.; Reimer, N.; Stassen, I.; Vermoortele, F.; Ameloot, R.; Stock, N.; Kirschhock, C. E. A.; De Vos, D. A zirconium squarate metal-organic framework with modulator-dependent molecular sieving properties. *Chem. Commun.* **2014**, *50* (70), 10055–10058.

(45) Cavka, J. H.; Jakobsen, S.; Olsbye, U.; Guillou, N.; Lamberti, C.; Bordiga, S.; Lillerud, K. P. A New Zirconium Inorganic Building Brick Forming Metal Organic Frameworks with Exceptional Stability. *J. Am. Chem. Soc.* **2008**, *130* (42), 13850–13851.

(46) Liu, J.; Redfern, L. R.; Liao, Y.; Islamoglu, T.; Atilgan, A.; Farha, O. K.; Hupp, J. T. Metal-Organic-Framework-Supported and -Isolated Ceria Clusters with Mixed Oxidation States. *ACS Appl. Mater. Interfaces* **2019**, *11* (51), 47822–47829.

(47) Yakovenko, A. A.; Wei, Z.; Wriedt, M.; Li, J.-R.; Halder, G. J.; Zhou, H.-C. Study of Guest Molecules in Metal-Organic Frame-

works by Powder X-ray Diffraction: Analysis of Difference Envelope Density. *Cryst. Growth Des.* **2014**, *14* (11), 5397–5407.

(48) Xu, D.; Hong, X.; Liu, G. Highly dispersed metal doping to ZnZr oxide catalyst for CO₂ hydrogenation to methanol: Insight into hydrogen spillover. *J. Catal.* **2021**, *393*, 207–214.

(49) Kouva, S.; Honkala, K.; Lefferts, L.; Kanervo, J. Review: monoclinic zirconia, its surface sites and their interaction with carbon monoxide. *Catal. Sci. Technol.* **2015**, *5* (7), 3473–3490.

(50) He, M.-Y.; Ekerdt, J. G. Infrared Studies of the Adsorption of Synthesis Gas on Zirconium Dioxide. *J. Catal.* **1984**, *87*, 381–388.

(51) Fisher, I. A.; Bell, A. T. In-Situ Infrared Study of Methanol Synthesis from H₂/CO₂ over Cu/SiO₂ and Cu/ZrO₂/SiO₂. *J. Catal.* **1997**, *172*, 222–237.

(52) Bianchi, D.; Chafik, T.; Khalfallah, M.; Teichner, S. J. Intermediate species on zirconia supported methanol aerogel catalysts. IV. Adsorption of carbon dioxide. *Appl. Catal., A* **1994**, *112* (2), 219–235.

(53) Fujita, S.; Usui, M.; Ito, H.; Takezawa, N. Mechanisms of Methanol Synthesis from Carbon Dioxide and from Carbon Monoxide at Atmospheric Pressure over Cu/ZnO. *J. Catal.* **1995**, *157*, 403–413.

(54) Fujita, S.; Usui, M.; Ohara, E.; Takezawa, N. Methanol synthesis from carbon dioxide at atmospheric pressure over Cu/ZnO catalyst. Role of methoxide species formed on ZnO support. *Catal. Lett.* **1992**, *13*, 349–358.

(55) Edwards, J. F.; Schrader, G. L. Methanol, formaldehyde, and formic acid adsorption on methanol synthesis catalysts. *J. Phys. Chem.* **1985**, *89* (5), 782–788.

(56) Wang, Y.; Gao, W.; Li, K.; Zheng, Y.; Xie, Z.; Na, W.; Chen, J. G.; Wang, H. Strong Evidence of the Role of H₂O in Affecting Methanol Selectivity from CO₂ Hydrogenation over Cu-ZnO-ZrO₂. *Chem.* **2020**, *6* (2), 419–430.

(57) Ueno, A.; Onishi, T.; Tamaru, K. Reaction Intermediates in Methyl Alcohol Decomposition on ZnO. *Trans. Faraday Soc.* **1971**, *67*, 3585–3589.